Simulating global and local surface temperature changes due to Holocene anthropogenic land cover change

Feng He,[1] Steve J. Vavrus,[1] John E. Kutzbach,[1] William F. Ruddiman,[2] Jed O. Kaplan,[3] and Kristen M. Krumhardt[3]

Received 24 September 2013; revised 4 December 2013; accepted 7 December 2013.

[1] Surface albedo changes from anthropogenic land cover change (ALCC) represent the second largest negative radiative forcing behind aerosol during the industrial era. Using a new reconstruction of ALCC during the Holocene era by Kaplan et al. (2011), we quantify the local and global temperature response induced by Holocene ALCC in the Community Climate System Model, version 4. We find that Holocene ALCC causes a global cooling of 0.17°C due to the biogeophysical effects of land-atmosphere exchange of momentum, moisture, and radiative and heat fluxes. On the global scale, the biogeochemical effects of Holocene ALCC from carbon emissions dominate the biogeophysical effects by causing 0.9°C global warming. The net effects of Holocene ALCC amount to a global warming of 0.73°C during the preindustrial era, which is comparable to the ~0.8°C warming during industrial times. On local to regional scales, such as parts of Europe, North America, and Asia, the biogeophysical effects of Holocene ALCC are significant and comparable to the biogeochemical effect.
Citation: He, F., S. J. Vavrus, J. E. Kutzbach, W. F. Ruddiman, J. O. Kaplan, and K. M. Krumhardt (2014), Simulating global and local surface temperature changes due to Holocene anthropogenic land cover change, *Geophys. Res. Lett.*, *41*, doi:10.1002/2013GL058085.

1. Introduction

[2] Humans have dramatically altered the Earth's surface through agriculture and industrial practices and transformed over half of natural biomes into anthropogenic biomes ("anthromes") [*Ellis et al*., 2010]. Anthropogenic land cover change (ALCC) influences global climate through both biogeophysical and biogeochemical feedbacks to the atmosphere. The biogeochemical effects of ALCC include emissions of greenhouse gases and aerosols from biomass burning, deforestation, rice cultivation, etc. The biogeophysical feedbacks include modification of the land-atmosphere exchange of momentum and moisture, as well as radiative and heat fluxes.

[3] Compared with studies of the global impact of the anthropogenic biogeochemical effect, e.g., the global mean temperature increase associated with the anthropogenic greenhouse gas increase, the level of scientific understanding of the biogeophysical effects of ALCC is still incomplete, with a negative radiation forcing of $-0.15 \pm 0.10\,\mathrm{W\,m^{-2}}$ summarized in the Intergovernmental Panel on Climate Change Fifth Assessment Report [*Stocker et al*., 2013]. Several challenges remain in order to reduce the uncertainty in the biogeophysical effects of ALCC.

[4] For example, unlike the well-mixed atmospheric greenhouse gases, ALCC is spatially heterogeneous [*Pitman et al*., 2012]. Published reconstructions of past ALCC vary widely in terms of both the timing and absolute magnitude of land use change [*Goldewijk*, 2001; *Kaplan et al*., 2011; *Pongratz et al*., 2008; *Ramankutty and Foley*, 1999]. Additionally, the consistent implementation of ALCC forcing into climate models remains a challenge because of the wide variety of land surface models and the different vegetation types that are parameterized in these models as well as different implementation strategies for ALCC [*Pitman et al*., 2009].

[5] Adding to these complications, the impact of ALCC on global climate is the net effect of often opposing forcings from biogeochemical and biogeophysical feedbacks [*Betts*, 2000; *Brovkin et al*., 2004; *Claussen et al*., 2001; *Matthews et al*., 2004; *Pongratz et al*., 2010], with biogeochemical effects subject to the climate sensitivity of individual climate models [*Bala et al*., 2007], while biogeophysical effects are subject to the often opposing effects of radiative, latent, and sensible heat fluxes that are not well constrained by the observations [*Davin and de Noblet-Ducoudre*, 2010; *Feddema et al*., 2005; *Pitman et al*., 2009]. With afforestation often being viewed as one of the strategies of mitigating ongoing global warming, all of the above challenges show that more research needs to done to guide the policies of carbon sequestration through ALCC [*Betts*, 2000; *Feddema et al*., 2005].

[6] Recently, several reconstructions of ALCC during the late Holocene have been published [*Goldewijk et al*., 2011; *Kaplan et al*., 2011; *Pongratz et al*., 2008]. All of these reconstructions were based on similar estimates of human population but differ in their assumptions regarding the relationship between population and land use. The HYDE data set [*Goldewijk et al*., 2011] assumes that throughout the Holocene, per capita land use remained close to the value recorded in Food and Agriculture Organization statistics in 1961 A.D. With the exponential rise in global populations during the second half of the twentieth century, this assumption results in very low levels of land use in most parts of the world before 1850 A.D. The *Pongratz et al*. [2008] data set, which covers the period 850–1850 A.D., uses a much more sophisticated methodology to estimate per capita land use, but the result is similar to HYDE, with little land use in most

[1]Center for Climatic Research, University of Wisconsin-Madison, Madison, Wisconsin, USA.
[2]Department of Environmental Sciences, University of Virginia, Charlottesville, Virginia, USA.
[3]Institute for Environmental Sciences, University of Geneva, Geneva, Switzerland.

Corresponding author: F. He, Center for Climatic Research, University of Wisconsin-Madison, 1225 W. Dayton St., Madison, WI 53706, USA. (fenghe@wisc.edu)

0094-8276/14/10.1002/2013GL058085

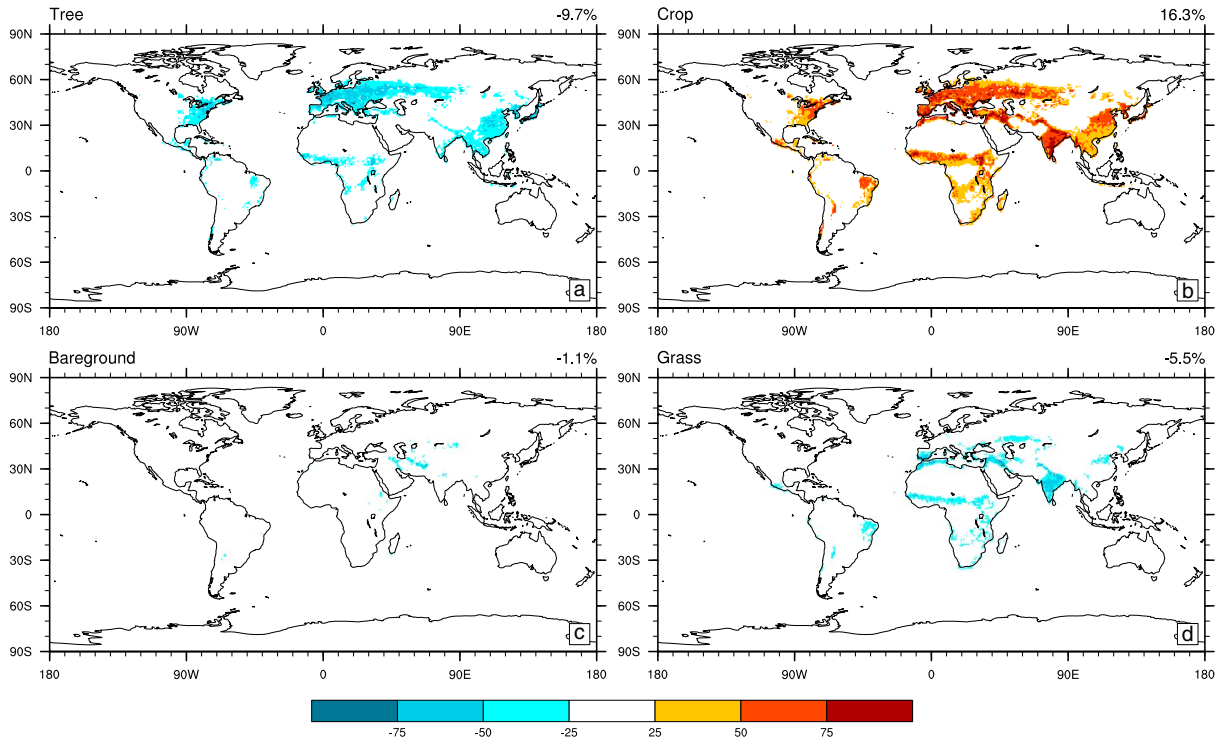

Figure 1. Holocene ALCC at 1850 A.D. shown as the difference between the KK10 reconstruction of land cover change and a map of potential natural vegetation [*Kaplan et al*., 2011]. The percentage change is based on the global land area, excluding both Greenland and Antarctica: (a) tree, (b) crop, (c) bareground, and (d) grass.

regions before 1850 A.D., particularly in the Western Hemisphere. The trend of per capita land use in KK10 data set [*Kaplan et al*., 2009, 2011] is based on the theory of agricultural intensification [*Boserup*, 1965; *Ellis et al*., 2013; *Ruddiman and Ellis*, 2009], whereby under low population pressure, humans used land extensively and with low labor input, and only intensified their land use under circumstances of land scarcity brought upon by high population densities [*Kaplan et al*., 2009]. As a result, the KK10 reconstruction shows that small populations resulted in large magnitudes of land use during the entire preindustrial Holocene, causing the total global ALCC at 1850 A.D. to be approximately twice as large as that in the HYDE or *Pongratz et al*. [2008] reconstructions [*Ellis et al*., 2013; *Kaplan et al*., 2011] (for a graphical comparison, see *Schmidt et al*. [2012], Figure 1).

[7] As a result, quantifying and understanding the differences among Holocene ALCC is one of the largest challenges in estimating climatic impacts of Holocene ALCC [*Ellis et al*., 2013]. For example, previous studies have shown that the biogeophysical feedback during the last millennium is much weaker than biogeochemical feedbacks on a global scale but can be as important as the biogeochemical effect on regional scales [e.g., *Pongratz et al*., 2010]. But, as noted above, this is based on an ALCC reconstruction that shows relatively low magnitudes of land use in preindustrial time.

[8] While regional studies have used KK10 to investigate the biogeophysical impacts of ALCC on climate [*Cook et al*., 2012; *Dermody et al*., 2012], no study to date has used the KK10 reconstruction to examine the relative importance of biogeophysical and biogeochemical feedbacks on global climate. In this study we assess the relative importance of biogeophysical and biogeochemical feedbacks to global climate by running the Community Climate System Model, version 4 (CCSM4) [*Gent et al*., 2011] in a series of experiments, driven by different levels of greenhouse gas concentrations, the KK10 ALCC scenario, and a control scenario with natural vegetation only. We further compare our results with previous model experiments that only considered biogeochemical feedbacks in Holocene climate change [*Kutzbach et al*., 2011; *Ruddiman*, 2003].

2. Model and Experiments

[9] All simulations were performed at 1° resolution with the CCSM4 slab-ocean model, which is the atmosphere-sea ice-land mixed-layer ocean configuration of CCSM4 [*Gent et al*., 2011]. The 1° resolution is considerably higher than those in previous land use simulations, which are around 3–4° in *Pitman et al*. [2009], *Davin and de Noblet-Ducoudre* [2010], and *Pongratz et al*. [2010]. The atmosphere model is the Community Atmosphere Model, version 4, with a finite volume dynamical core and 26 layers in the vertical direction [*Neale et al*., 2013]. The sea ice model is the version 4 of the Los Alamos National Laboratory sea ice model (CICE4) [*Holland et al*., 2012]. The land model is the Community Land Model, version 4 (CLM4) [*Lawrence et al*., 2012], with a carbon-nitrogen cycle model that is prognostic in carbon/nitrogen and vegetation phenology [*Thornton et al*., 2007]. CLM4 includes 14 natural plant functional types (PFTs) with eight tree PFTs, three shrub PFTs, and three grass PFTs, plus one crop PFT and bareground [*Lawrence and Chase*, 2007; *Oleson et al*., 2010]. Compared with previous versions, CLM4 more realistically simulates snow cover, soil temperatures in organic-rich soils, and extensive areas with

Table 1. Simulations of Biogeophysical and Biogeochemical Effects of Holocene ALCC

	KK10 PFT reconstructions	Greenhouse gases
	Biogeophysical effect	
Biogeophysical run	1850 A.D.	1850 A.D.
Control run	Natural vegetation[a]	1850 A.D.
	Biogeochemical effect	
Biogeochemical run	1850 A.D.	NA
Control run	1850 A.D.	1850 A.D.

[a]The one natural vegetation reconstruction used throughout the Holocene, to compare with ALCC, follows the established methodology of *Kaplan et al*. [2011]. This one natural vegetation reference is obtained by running a dynamic vegetation model forced by modern-day observations and then regrouping the results as PFTs corresponding to CCSM4 PFTs. This methodology has the practical advantage of having only one natural baseline against which to calculate ALCC through time, and no alternative natural global-scale baseline is available or accepted as an alternative.

near-surface permafrost [*Lawrence et al*., 2012]. The initial conditions of all experiments were from the 1° CCSM4 slab-ocean control simulation for preindustrial period (~1850 A.D.).

[10] We performed four experiments with CCSM4 to quantify biogeophysical and biogeochemical feedbacks (Table 1): two experiments to quantify the magnitude of ALCC-induced biogeophysical feedbacks and two to examine the effects of changing greenhouse concentrations. The two experiments for biogeophysical effects differed only in the distribution of PFTs that were input to CLM4, which had its dynamic vegetation option turned off. The ALCC simulation used the KK10 land use map at 1850 A.D., and our control simulation used a reconstruction of potential natural vegetation [*Kaplan et al*., 2011]. In CLM4, two types of crops are allowed to account for the different physiology of crops, but currently, only the first crop type is specified in the surface data set [*Oleson et al*., 2010]. The KK10 fraction of used land was used to specify the fractional coverage of the crop PFT; the fractional coverage of all of the other PFTs within a model grid cell was scaled accordingly to preserve their relative proportions. The maps of natural vegetation were derived from Lund-Potsdam-Jena Dynamic Global Vegetation Model (LPJ DGVM) output [*Sitch et al*., 2003]. PFT cover fractions were then regrouped into PFT categories used by CCSM. The two experiments for biogeochemical effects differed only in the prescribed greenhouse gas concentrations (Table 2). The greenhouse gas values for Experiment PI (preindustrial period) were adopted from the National Center for Atmospheric Research (NCAR) CCSM4 preindustrial control simulation [*Gent et al*., 2011]. The greenhouse gas values for Experiment NA (no anthropogenic carbon emission) were adopted from *Kutzbach et al*. [2011], which are based on linear projection from earlier Holocene trends and coincide with the observed values during stage 19, the closest analog to the Holocene among previous interglacials based on the insolation variations [*Tzedakis et al*., 2012]. The experiments for biogeophysical and biogeochemical effects were run for 110 and 135 years, respectively, with the annual mean averages of the last 50 years used for comparisons.

3. Results

[11] In the KK10 scenario, land use at 1850 A.D. was concentrated in southeast North America, parts of Central America, most of Europe south of 60°N, the western portion of North Asia, southeast China, mainland Southeast Asia, India, areas surrounding the tropical rainforest in Africa, southern Africa, and northeast Brazil (Figure 1b). In those regions, 25%–75% of natural vegetation had been converted into crops by 1850 A.D. The total amount of land under human use in 1850 A.D. was approximately 22 million km^2, or 16.3% global land area. Of this total, 60% was land that would naturally be forest and 33% would naturally be grassland (Figures 1a and 1d).

4. Biogeophysical Effects

[12] In the 1° CCSM4 slab-ocean simulation, the biogeophysical effect of Holocene ALCC causes broad cooling in the midlatitudes of the Northern Hemisphere and scattered warming in mainland Southeast Asia, India, and in areas surrounding the tropical rainforest of Africa (Figure 2a). Overall, the global climate response to the biogeophysical effect of Holocene ALCC is a cooling of 0.17°C, which is fivefold larger than the 0.03°C cooling caused by the biogeophysical effect of ALCC during the last millennium estimated by *Pongratz et al*. [2010] in low-resolution ECHAM5. As noted above, the *Pongratz et al*. [2010] scenario has relatively low amounts of land use at 1850 A.D. compared to KK10, particularly in the Western Hemisphere.

[13] The broad cooling in the midlatitudes of the Northern Hemisphere is caused by increased albedo after deforestation. Since forests have lower surface albedo than cropland and can mask the high albedo of underlying snow, deforestation over North America, Europe, and China results in a widespread increase of surface albedo of 0.01–0.05 across Northern Hemisphere midlatitudes (Figure 3a). As a result, the net solar radiation flux at the surface is reduced by 2–8 W/m^2 in these regions (Figure 4a), and this decrease causes a widespread cooling of 0.25 to over 1°C in the midlatitude Northern Hemisphere (Figure 2a). The largest cooling (over 1°C) occurs locally where deforestation is greatest in North America and Europe (Figures 1a and 2a), but a significant cooling of over 0.5°C also occurs remotely over the North Atlantic and Asia, which are downwind of the largest ALCC over North America and Europe, respectively. The surface cooling in the midlatitude Northern Hemisphere causes less loss of surface sensible heat (Figure 4c), which partly compensates the loss of the net surface solar radiation absorption caused by the increase of the surface albedo.

[14] Simulated albedo changes from Holocene ALCC are mostly confined to the midlatitudes of the Northern Hemisphere. For the land area of the tropics and Southern Hemisphere, surface temperature changes are mainly caused by the changes of the total leaf area index (LAI) resulting from

Table 2. Greenhouse Gases in Biogeochemical Simulations[a]

Greenhouse gases	CO_2 (ppm)	CH_4 (ppb)	N_2O (ppb)	CFC11 (ppt)	CFC12 (ppt)
PI	284.7	791.6	275.68	12.48	0
NA	245	445	270	0	0
NA-PI radiative forcing (W/m^2)	0.804	0.225	0.019	0.003	0.000

[a]Total radiative forcing from NA (no anthropogenic carbon emission) to PI (preindustrial period, ~1850 A.D.): 1.05 W/m^2. The PI greenhouse gas values were adopted from NCAR CCSM4 PI control simulation [*Gent et al*., 2011]. The NA greenhouse gas values were adopted from *Kutzbach et al*. [2011] with minor revision from updated ice core data.

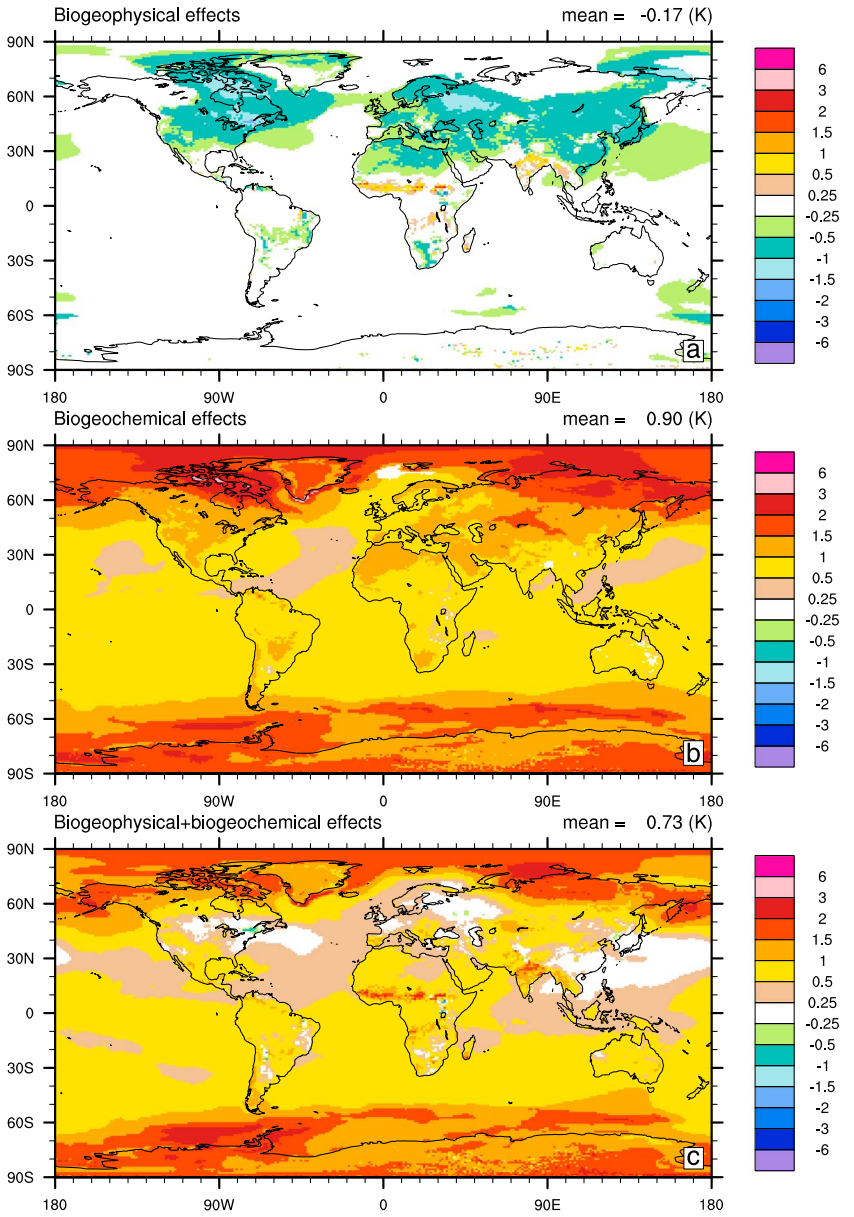

Figure 2. Simulated surface temperature changes due to (a) biogeophysical effects based on Holocene ALCC at 1850 A.D., (b) biogeochemical effects based on differences of greenhouse gas forcing between 1850 A.D. and NA (no anthropogenic carbon emission), and (c) net effects of Holocene ALCC (biophysical effects + biogeochemical effects). Values which do not pass a revised Student's *t* test [*Zwiers and von Storch*, 1995] at 95% confidence have been omitted.

Holocene ALCC (Figure 3b). The LAI changes can modify the surface latent heat fluxes through the changes of evapotranspiration (Figure 4d). For example, in the Southern Hemisphere, there is scattered cooling in northeast Brazil and southern Africa (Figure 2a). These regions are not associated with increased surface albedo but rather with an increase in the total leaf area index (LAI) (Figures 3a and 3b), which is mostly due to the conversion of deciduous forests and semiarid areas to croplands (Figure 1b). LAI increases also occur in the Northern Hemisphere, such as the southeast U.S., westernmost Europe, and southeastern China. In all of the above five regions, the LAI increase causes an increase of latent heat release due to increased evapotranspiration (Figure 4d), resulting in local cooling that is more discernible in the Southern Hemisphere. On the other hand, increased evapotranspiration also causes increases in local clouds in all of these aforementioned regions except southeastern China (Figure 3c). More clouds reduce the net absorption of solar radiation at the surface (Figure 4a). Surface heat flux loss from reduced solar radiation and enhanced latent heat flux is balanced by the reduction of heat flux loss from net longwave and sensible heat due to increases in clouds and surface cooling (Figures 4b and 4c). In the tropics, land use reduces LAI in India, mainland Southeast Asia, and areas surrounding the tropical rainforests in Africa as a result of the conversion of tropical rainforests into cropland (Figure 3b). The reduction of evapotranspiration and cloud cover in these regions results in less latent heat flux loss, more solar radiation absorption (Figures 3c, 4a and 4d), and subsequent surface warming over these regions (Figure 2a).

[15] In summary, the simulated biogeophysical effects of Holocene ALCC on surface temperature in a 1° CCSM4

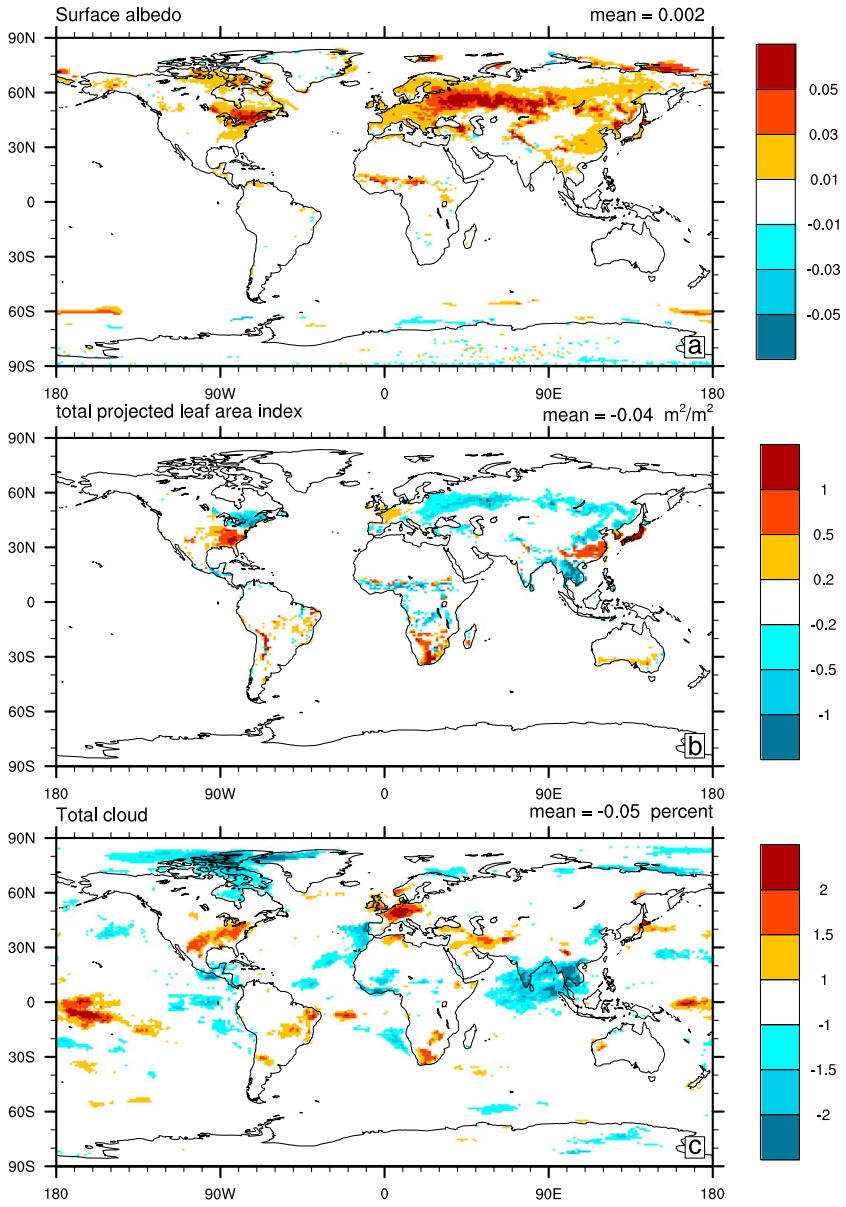

Figure 3. Simulated annual-mean changes of (a) surface albedo, (b) LAI, and (c) total cloud over land due to the biogeophysical effect of Holocene ALCC in CCSM4. Values which do not pass a revised Student's *t* test at 95% confidence have been omitted.

slab-ocean simulation (Figure 2a) are consistent with previous low-resolution simulations [e.g., *Davin and de Noblet-Ducoudre*, 2010]. Prominent cooling in Northern Hemisphere midlatitudes results from increased albedo from deforestation (Figure 3a). Also discernible, but scattered, is surface warming in the tropics caused by reduced latent heat loss due to lower LAI values after deforestation (Figure 3b). Our 1° CCSM4 slab-ocean model results also show that the cloud response to changes of LAI helps to amplify the surface temperature response to changes of latent heat loss in the subtropics and tropics (Figure 3c).

5. Biogeochemical Effects

[16] According to the early anthropogenic hypothesis, atmospheric CO_2, CH_4, and N_2O concentrations should have fallen to ~245 ppm, ~445 ppb, and ~270 ppb, respectively, by 1850 A.D., consistent with decreases observed at similar times in previous (natural) interglaciations [*Ruddiman*, 2003, 2007]. Instead, emissions from agriculture resulted in CO_2, CH_4, and N_2O concentrations of ~285 ppm, ~790 ppb, and ~275 ppb, respectively (Table 2). The total radiative forcing from the greenhouse gas increase is 1.05 W/m^2, which causes global surface temperature to increase by 0.90°C in the 1° CCSM4 slab-ocean simulation (Figure 2b). This translates into a climate sensitivity of 3.2°C (3.2°C global temperature increase per doubling of atmospheric CO_2). *Bitz et al*. [2012] obtained the same climate sensitivity in a 1° CCSM4 slab-ocean simulation based on doubling CO_2 experiments with CO_2 concentrations of 285 and 570 ppm.

[17] The spatial pattern of the temperature response exhibits the classic feature of polar amplification, with a 0.5–1°C temperature increase in low latitudes and over 1.5°C in polar regions. The minimum temperature increase occurs in

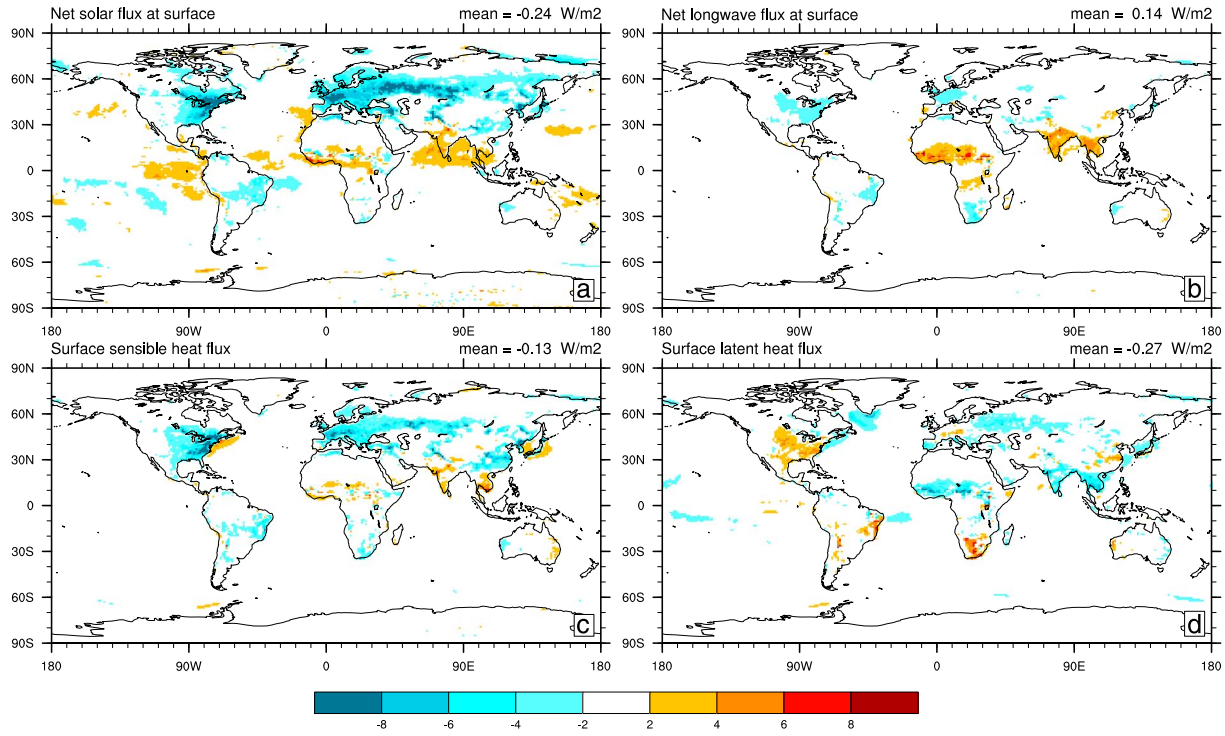

Figure 4. Simulated annual-mean changes of net flux of shortwave and longwave radiation as well as sensible and latent heat flux at surface due to the biogeophysical effect of Holocene ALCC. Values which do not pass a revised Student's *t* test at 95% confidence have been omitted.

the tropical North Atlantic and tropical North Pacific Oceans, with less than 0.5 °C warming. The net biogeophysical and biogeochemical effects of Holocene ALCC on the global mean temperature is 0.73°C warming (Figure 2c) or approximately 80% as large as the biogeochemical effect alone (Figure 2b). The pattern of the net global temperature response still shows a polar amplification effect, but the widespread warming of more than 2°C over the Arctic in the experiments for biogeochemical effects is greatly reduced to below 2°C. Furthermore, the net temperature response in the regions of major Holocene deforestation, such as eastern North America, Europe, and southeast China, does not exhibit discernible warming, nor does the temperature response downwind from these regions, such as parts of the North Atlantic and North Pacific Ocean. In these regions, the cooling by the biogeophysical effect of Holocene ALCC is comparable to the warming of the biogeochemical effect. On the other hand, warming from the biogeophysical effect of Holocene ALCC in the tropics amplifies the warming from the biogeochemical effects and produces some hot spots with over 1.5°C warming in northern India and areas surrounding the tropical rainforest in Africa (Figure 2c).

6. Discussion

[18] Our experiments with CCSM4 and different land use and greenhouse gas forcing show that biogeophysical feedbacks of Holocene ALCC caused a global cooling of 0.17°C, while biogeochemical feedbacks caused a 0.90°C global warming. Therefore, at 1850 A.D. the biogeochemical effects of land use were a factor of 5 more important than the biogeophysical effects on the global scale, even when using the KK10 scenario, which may be considered an upper bound estimate of the magnitude of land use. We note that the biogeochemical effects of Holocene ALCC might be reduced by anthropogenic aerosol emissions [*Hansen et al.*, 2007], and on local to regional scales, such as parts of southeast North America, Europe, and southeast China, the biogeophysical effects of Holocene ALCC induce prominent cooling due to albedo increases from deforestation and are able to reduce or cancel regional warming caused by biogeochemical feedbacks. We also note that this study does not address the timing of global and regional effects of Holocene ALCC, which will be addressed in our upcoming research.

[19] The net effect of Holocene ALCC amounts to a global warming of 0.73°C during the preindustrial era in our simulations (Figure 2c) and is comparable to the ~0.8°C warming during industrial time [*Hansen et al.*, 2010]. The lack of ocean dynamics in the 1° CCSM4 slab-ocean simulations could underestimate the climate sensitivity because of the lack of feedbacks from ocean heat transport [*Kutzbach et al.*, 2013; *Manabe and Bryan*, 1985]. In 1° CCSM4 fully coupled simulations, the climate sensitivity is ~65% larger than the 1° CCSM4 slab-ocean simulations during the Holocene (5.3°C versus 3.2°C) [*Kutzbach et al.*, 2013]. With this greater climate sensitivity, we could speculate that the biogeochemical effects of Holocene ALCC could have caused a global warming of ~1.5°C, and the net biogeophysical and biogeochemical effects of Holocene ALCC could cause a global warming of 1.2 °C during the preindustrial era in our simulations, which is 50% higher than the global warming of ~0.8°C during industrial times. Therefore, the net effects of Holocene ALCC support the central theme of the early anthropogenic hypothesis that the human impact on global climate started thousands of years before the Industrial Revolution as a result of the greenhouse

gas emissions caused by farming activities such as deforestation and rice cultivation [*Ruddiman*, 2003, 2007, 2013].

[20] **Acknowledgments.** This work was supported by National Science Foundation grants ATM-0602270, ATM-0902802, and AGS-1203430 to the University of Wisconsin-Madison and ATM-0902982 and AGS-1203965 to the University of Virginia. Computational support was provided by NCAR's Climate Simulation Laboratory, which is supported by the National Science Foundation. We appreciate the discussions with Erle Ellis. This is CCR contribution no. 1167.

[21] The Editor thanks two anonymous reviewers for their assistance in evaluating this paper.

References

Bala, G., K. Caldeira, M. Wickett, T. J. Phillips, D. B. Lobell, C. Delire, and A. Mirin (2007), Combined climate and carbon-cycle effects of large-scale deforestation, *Proc. Natl. Acad. Sci. U. S. A.*, *104*(16), 6550–6555.

Betts, R. A. (2000), Offset of the potential carbon sink from boreal forestation by decreases in surface albedo, *Nature*, *408*(6809), 187–190.

Bitz, C. M., K. M. Shell, P. R. Gent, D. A. Bailey, G. Danabasoglu, K. C. Armour, M. M. Holland, and J. T. Kiehl (2012), Climate Sensitivity of the Community Climate System Model, Version 4, *J. Clim.*, *25*(9), 3053–3070.

Boserup, E. (1965), *The Conditions of Agricultural Growth: The Economics of Agrarian Change Under Population Pressure*, Aldine Pub. Co., Chicago.

Brovkin, V., S. Sitch, W. von Bloh, M. Claussen, E. Bauer, and W. Cramer (2004), Role of land cover changes for atmospheric CO_2 increase and climate change during the last 150 years, *Global Change Biol.*, *10*(8), 1253–1266.

Claussen, M., V. Brovkin, and A. Ganopolski (2001), Biogeophysical versus biogeochemical feedbacks of large-scale land cover change, *Geophys. Res. Lett.*, *28*(6), 1011–1014.

Cook, B. I., K. J. Anchukaitis, J. O. Kaplan, M. J. Puma, M. Kelley, and D. Gueyffier (2012), Pre-Columbian deforestation as an amplifier of drought in Mesoamerica, *Geophys. Res. Lett.*, *39*, L16706, doi:10.1029/2012GL052565.

Davin, E. L., and N. de Noblet-Ducoudre (2010), Climatic impact of global-scale deforestation: Radiative versus nonradiative processes, *J. Clim.*, *23*(1), 97–112.

Dermody, B. J., H. J. de Boer, M. F. P. Bierkens, S. L. Weber, M. J. Wassen, and S. C. Dekker (2012), A seesaw in Mediterranean precipitation during the Roman period linked to millennial-scale changes in the North Atlantic, *Clim. Past*, *8*(2), 637–651.

Ellis, E. C., K. K. Goldewijk, S. Siebert, D. Lightman, and N. Ramankutty (2010), Anthropogenic transformation of the biomes, 1700 to 2000, *Global Ecol. Biogeogr.*, *19*(5), 589–606.

Ellis, E. C., J. O. Kaplan, D. Q. Fuller, S. Vavrus, K. Klein Goldewijk, and P. H. Verburg (2013), Used planet: A global history, *Proc. Natl. Acad. Sci. U S A*, *110*(20), 7978–7985.

Feddema, J. J., K. W. Oleson, G. B. Bonan, L. O. Mearns, L. E. Buja, G. A. Meehl, and W. M. Washington (2005), The importance of land-cover change in simulating future climates, *Science*, *310*(5754), 1674–1678.

Gent, P. R., et al. (2011), The Community Climate System Model Version 4, *J. Clim.*, *24*(19), 4973–4991.

Goldewijk, K. K. (2001), Estimating global land use change over the past 300 years: The HYDE database, *Global Biogeochem. Cycles*, *15*(2), 417–433.

Goldewijk, K. K., A. Beusen, G. van Drecht, and M. de Vos (2011), The HYDE 3.1 spatially explicit database of human-induced global land-use change over the past 12,000 years, *Global Ecol. Biogeogr.*, *20*(1), 73–86.

Hansen, J., M. Sato, P. Kharecha, G. Russell, D. W. Lea, and M. Siddall (2007), Climate change and trace gases, *Philos. Trans. Ser. A Math. Phys. Eng. Sci.*, *365*(1856), 1925–1954.

Hansen, J., R. Ruedy, M. Sato, and K. Lo (2010), Global surface temperature change, *Rev. Geophys.*, *48*, RG4004, doi:10.1029/2010RG000345.

Holland, M. M., D. A. Bailey, B. P. Briegleb, B. Light, and E. Hunke (2012), Improved sea ice shortwave radiation physics in CCSM4: The impact of melt ponds and aerosols on Arctic sea ice, *J. Clim.*, *25*(5), 1413–1430.

Kaplan, J. O., K. M. Krumhardt, and N. Zimmermann (2009), The prehistoric and preindustrial deforestation of Europe, *Quat. Sci. Rev.*, *28*(27-28), 3016–3034.

Kaplan, J. O., K. M. Krumhardt, E. C. Ellis, W. F. Ruddiman, C. Lemmen, and K. K. Goldewijk (2011), Holocene carbon emissions as a result of anthropogenic land cover change, *Holocene*, *21*(5), 775–791.

Kutzbach, J. E., S. J. Vavrus, W. F. Ruddiman, and G. Philippon-Berthier (2011), Comparisons of atmosphere-ocean simulations of greenhouse gas-induced climate change for pre-industrial and hypothetical 'no-anthropogenic' radiative forcing, relative to present day, *Holocene*, *21*(5), 793–801.

Kutzbach, J. E., F. He, S. J. Vavrus, and W. F. Ruddiman (2013), The dependence of equilibrium climate sensitivity on climate state: Applications to studies of climates colder than present, *Geophys. Res. Lett.*, *40*, 3721–3726, doi:10.1002/grl.50724.

Lawrence, D. M., K. W. Oleson, M. G. Flanner, C. G. Fletcher, P. J. Lawrence, S. Levis, S. C. Swenson, and G. B. Bonan (2012), The CCSM4 land simulation, 1850–2005: Assessment of surface climate and new capabilities, *J. Clim.*, *25*(7), 2240–2260.

Lawrence, P. J., and T. N. Chase (2007), Representing a new MODIS consistent land surface in the Community Land Model (CLM 3.0), *J. Geophys. Res.*, *112*, G01023, doi:10.1029/2006JG000168.

Manabe, S., and K. Bryan (1985), CO_2-induced change in a coupled ocean-atmosphere model and its paleoclimatic implications, *J. Geophys. Res.*, *90*(Nc6), 1689–1707.

Matthews, H. D., A. J. Weaver, K. J. Meissner, N. P. Gillett, and M. Eby (2004), Natural and anthropogenic climate change: Incorporating historical land cover change, vegetation dynamics and the global carbon cycle, *Clim. Dyn.*, *22*(5), 461–479.

Neale, R. B., J. Richter, S. Park, P. H. Lauritzen, S. J. Vavrus, P. J. Rasch, and M. Zhang (2013), The Mean Climate of the Community Atmosphere Model (CAM4) in forced SST and fully coupled experiments, *J. Clim.*, *26*(14), 5150–5168.

Oleson, K. W., D. M. Lawrence, G. B. Bonan, M. G. Flanner, E. Kluzek, P. J. Lawrence, S. Levis, S. C. Swenson, and P. E. Thornton (2010), Technical description of version 4.0 of the Community Land Model (CLM), NCAR Technical Note.

Pitman, A. J., et al. (2009), Uncertainties in climate responses to past land cover change: First results from the LUCID intercomparison study, *Geophys. Res. Lett.*, *36*, L14814, doi:10.1029/2009GL039076.

Pitman, A.J., A. Arneth, L. Ganzeveld, 2012, Regionalizing global climate models, *Int. J. Climatol.*, *32*, 321–337, doi: 10.1002/joc.2279.

Pongratz, J., C. Reick, T. Raddatz, and M. Claussen (2008), A reconstruction of global agricultural areas and land cover for the last millennium, *Global Biogeochem. Cycles*, *22*, GB3018, doi:10.1029/2007GB003153.

Pongratz, J., C. H. Reick, T. Raddatz, and M. Claussen (2010), Biogeophysical versus biogeochemical climate response to historical anthropogenic land cover change, *Geophys. Res. Lett.*, *37*, L08702, doi:10.1029/2010GL043010.

Ramankutty, N., and J. A. Foley (1999), Estimating historical changes in global land cover: Croplands from 1700 to 1992, *Global Biogeochem. Cycles*, *13*(4), 997–1027.

Ruddiman, W. F. (2003), The anthropogenic greenhouse era began thousands of years ago, *Clim. Change*, *61*(3), 261–293.

Ruddiman, W. F. (2007), The early anthropogenic hypothesis: Challenges and responses, *Rev. Geophys.*, *45*, RG4001, doi:10.1029/2006RG000207.

Ruddiman, W. F. (2013), The Anthropocene, *Annu. Rev. Earth Planet. Sci.*, *41*(1), 45–68.

Ruddiman, W. F., and E. C. Ellis (2009), Effect of per-capita land use changes on Holocene forest clearance and CO_2 emissions, *Quat. Sci. Rev.*, *28*(27-28), 3011–3015.

Schmidt, G. A., et al. (2012), Climate forcing reconstructions for use in PMIP simulations of the Last Millennium (v1.1), *Geosci. Model Dev.*, *5*(1), 185–191.

Sitch, S., et al. (2003), Evaluation of ecosystem dynamics, plant geography and terrestrial carbon cycling in the LPJ dynamic global vegetation model, *Global Change Biol.*, *9*(2), 161–185.

Stocker, T. F., D. Qin, G. K. Plattner, M. Tignor, S. K. Allen, J. Boschung, A. Nauels, Y. Xia, V. Bex, and P. M. Midgley (Eds.) (2013), IPCC, 2013: Summary for policymakers, in *Climate Change 2013: The Physical Science Basis. Contribution of Working Group I to the Fifth Assessment Report of the Intergovernmental Panel on Climate Change*, pp. 1–27, Cambridge Univ. Press, Cambridge, U.K., and New York.

Thornton, P. E., J. F. Lamarque, N. A. Rosenbloom, and N. M. Mahowald (2007), Influence of carbon-nitrogen cycle coupling on land model response to CO_2 fertilization and climate variability, *Global Biogeochem. Cycles*, *21*, GB4018, doi:10.1029/2006GB002868.

Tzedakis, P. C., J. E. T. Channell, D. A. Hodell, H. F. Kleiven, and L. C. Skinner (2012), Determining the natural length of the current interglacial, *Nat. Geosci.*, *5*(2), 138–141.

Zwiers, F. W., and H. von Storch (1995), Taking serial correlation into account in tests of the mean, *J. Clim.*, *8*(2), 336–351.